Supporting Information for the manuscript:

Ligand and Electronic Effects on Copper-Arylnitroso Self-Assembly

F. Effaty, J. Zsombor-Pindera, A. Kazakova, B. Girard, M. S. Askari, and X. Ottenwaelder✉

Department of Chemistry and Biochemistry Concordia University, 7141 Sherbrooke Street West, Montreal, H4B 1R6, Canada

✉ Corresponding author. Tel.: +1-514-848-2424 x 8934; fax: +1-514-848-2424 x 2868; e-mail: dr.x@concordia.ca

Contents

1. Examples of UV-vis multivariate fitting

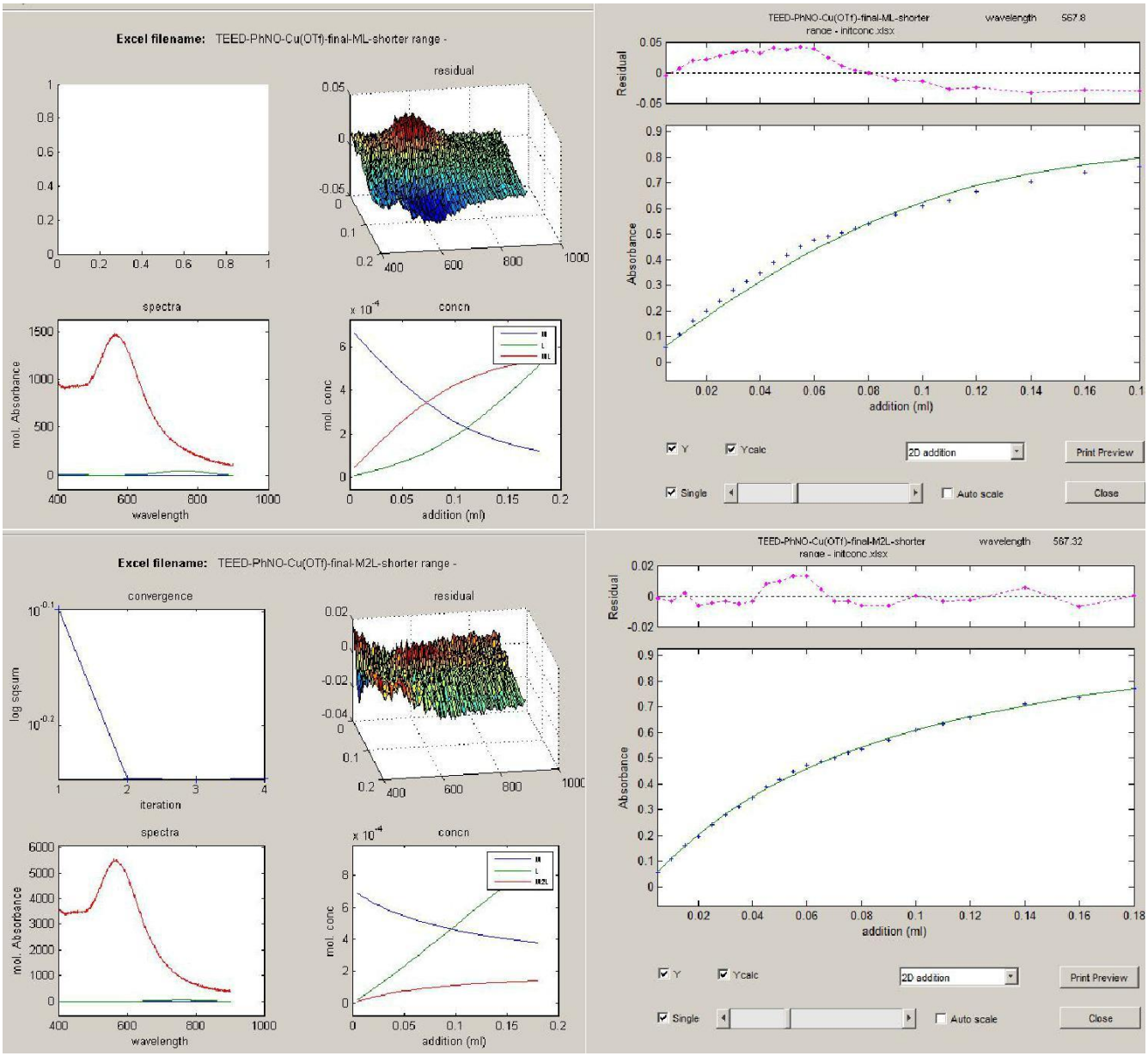

Figure S1. Screenshots of the fitting process with ReactLab™ Equilibria for **TEED-H**: (top) 1:1 Cu:ArNO model (bottom) 2:1 Cu:ArNO model.

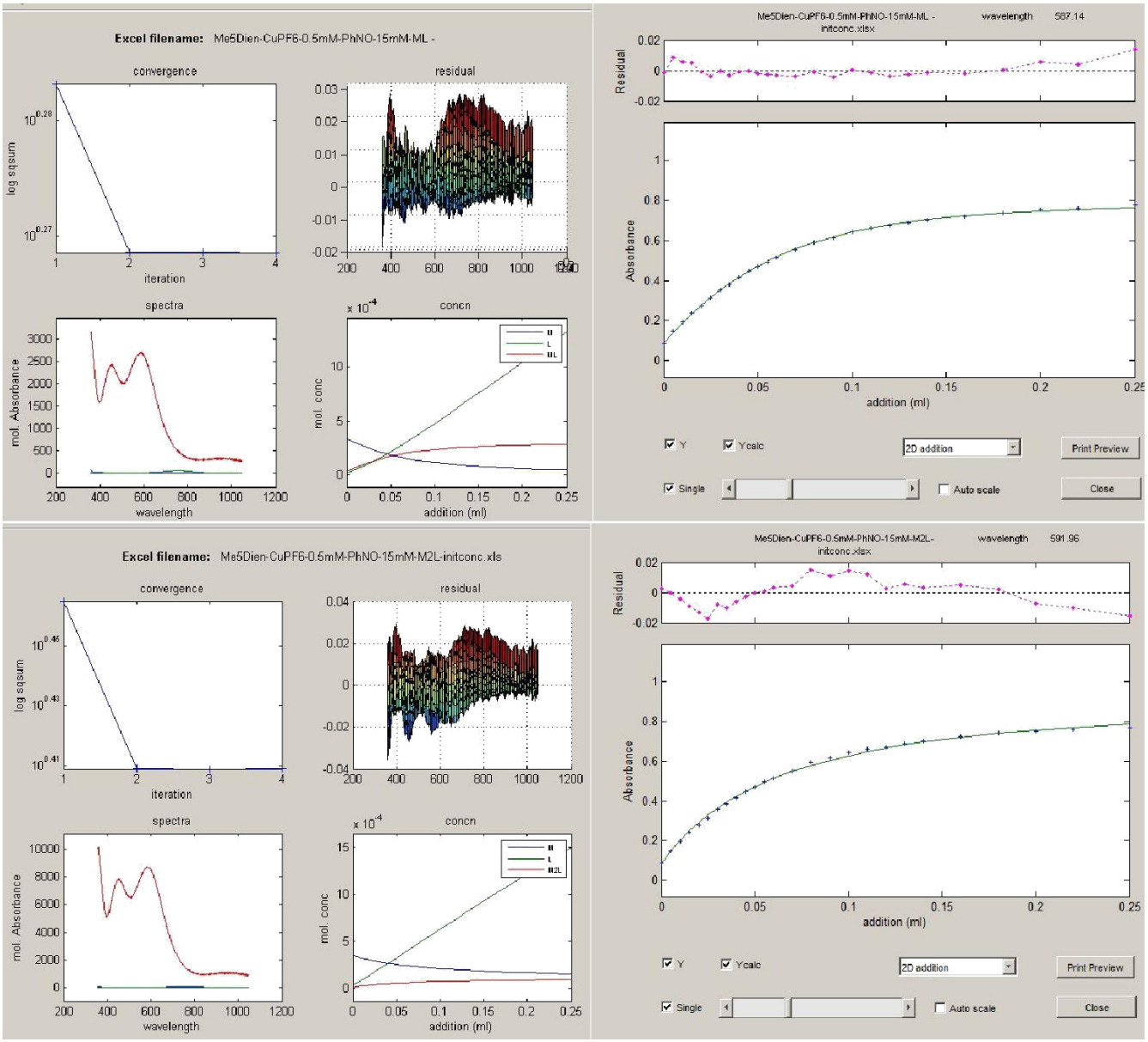

Figure S2. Screenshots of the fitting process with ReactLab™ Equilibria for **Me5DIEN-H**: (top) 1:1 Cu:ArNO model (bottom) 2:1 Cu:ArNO model.

2. Selection of NMR spectra

2.1. DBED-Z species

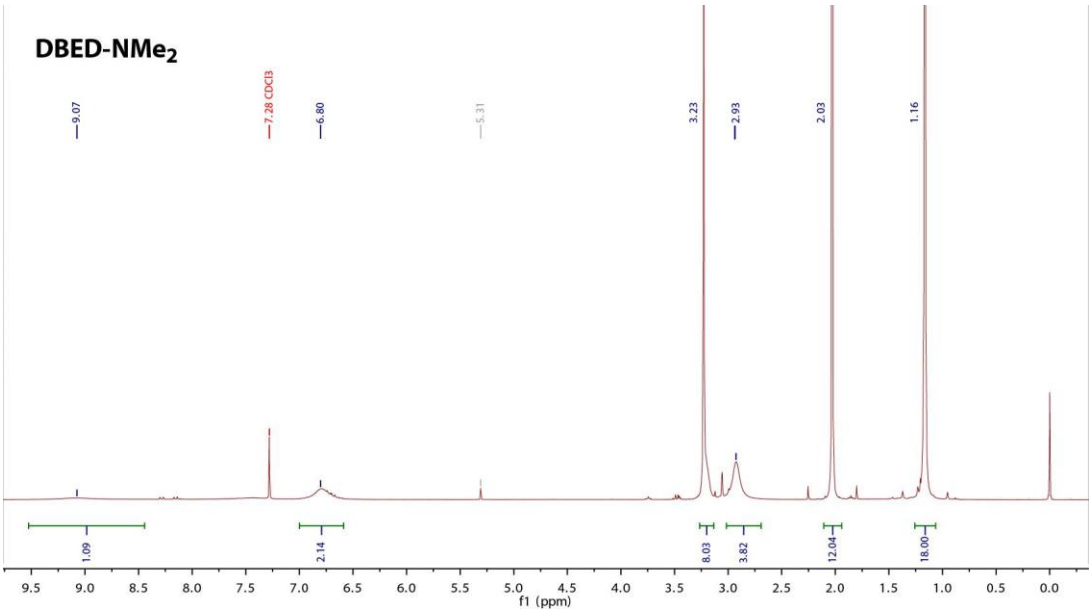

Figure S3. ^{1}H-NMR (500 MHz) spectra of **DBED-NMe2** formed in situ in $CDCl_3$ at 23°C.

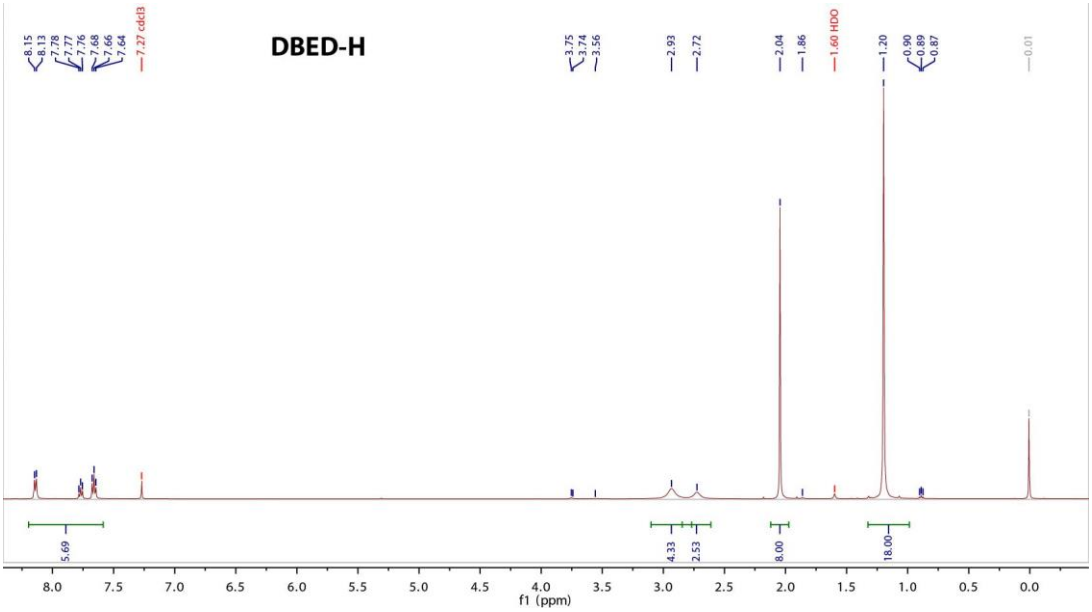

Figure S4. ^{1}H-NMR (500 MHz) spectra of **DBED-H** formed in situ in $CDCl_3$ at 23°C.

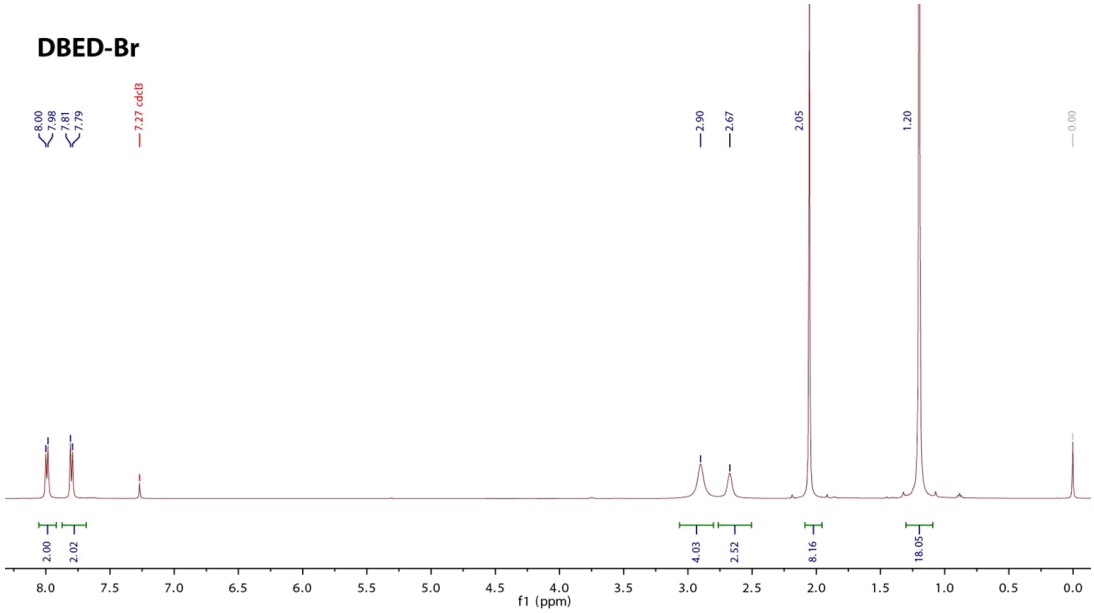

Figure S5. ^{1}H-NMR (500 MHz) spectra of **DBED-Br** formed in situ in $CDCl_3$ at 23°C.

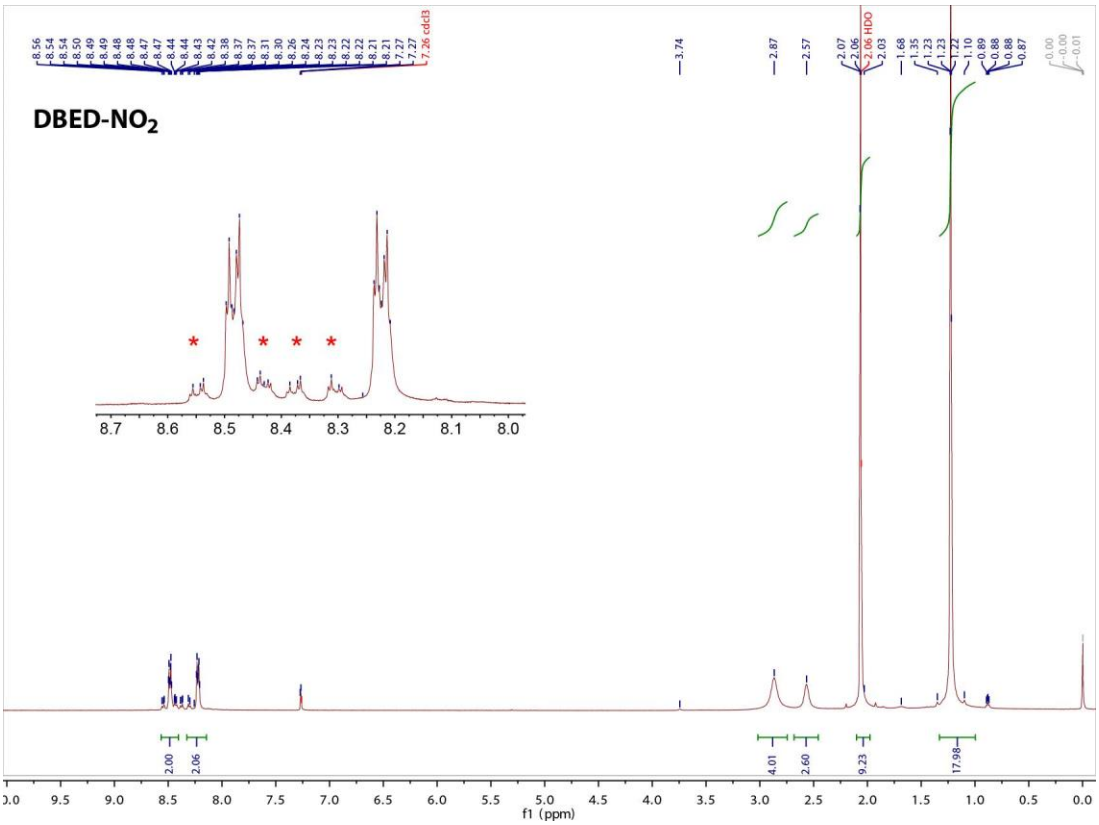

Figure S6. ^{1}H-NMR (500 MHz) spectra of **DBED-NO_2** formed in situ in d^6-acetone at 23°C. The red * in the inset denote the azozy decomposition product.

2.2. TEED-Z species

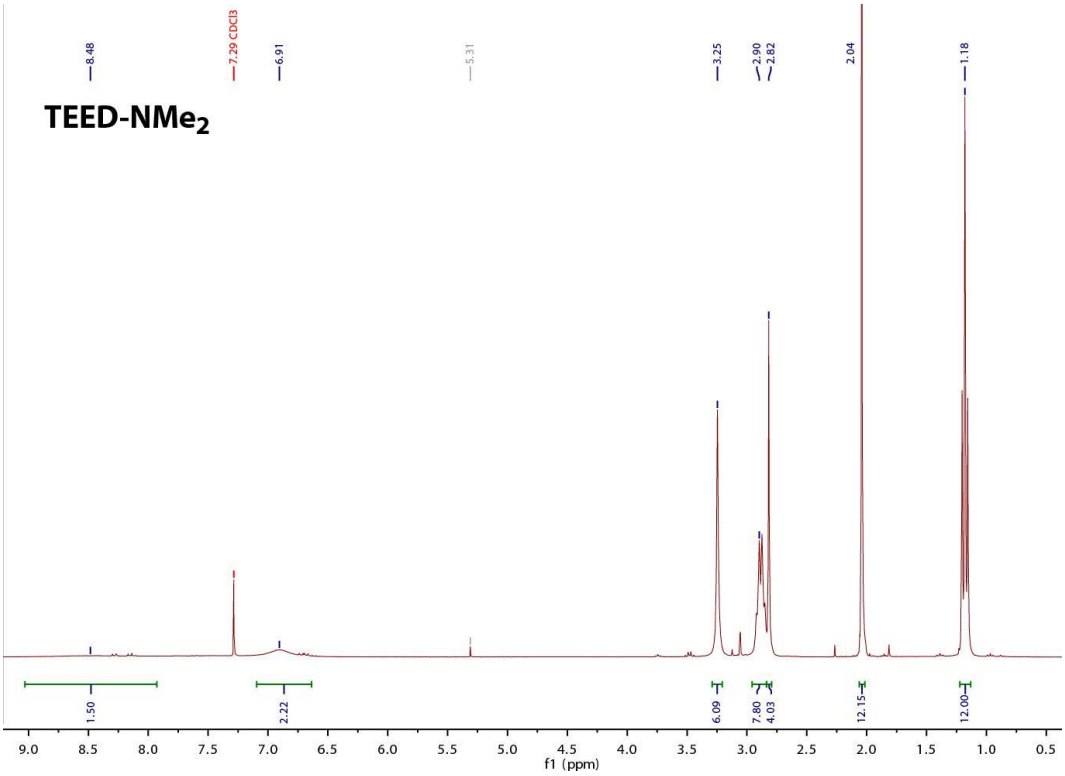

Figure S7. ^{1}H-NMR (500 MHz) spectra of **TEED-NMe$_2$** formed in situ in $CDCl_3$ at 23°C.

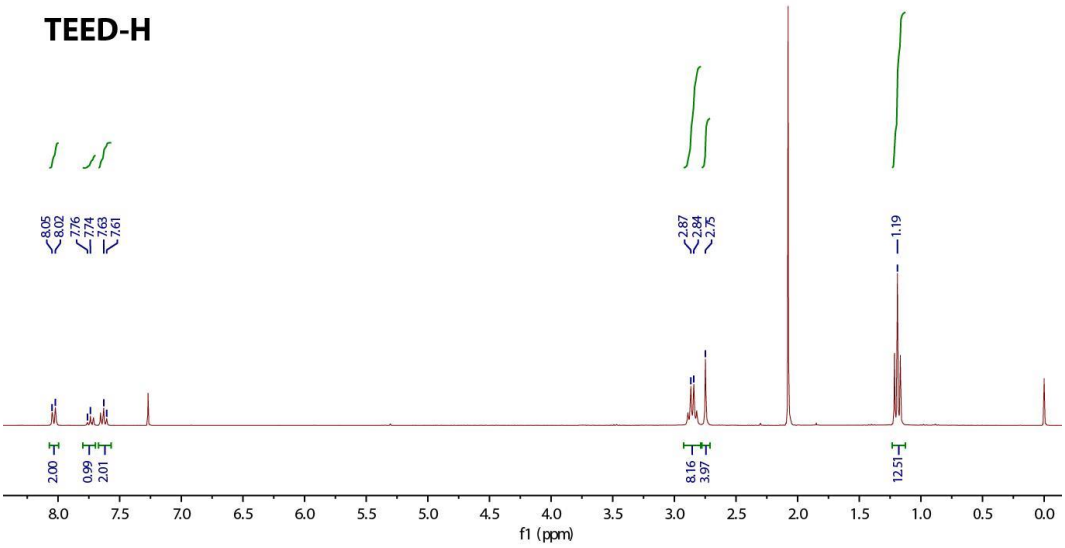

Figure S8. ^{1}H-NMR (300 MHz) spectra of **TEED-H** formed in situ from a 1:1 TEEDCu^{I}:^{H}ArNO stoichiometry in $CDCl_3$ at 23°C.

2.3. Me_5DIEN-Z species

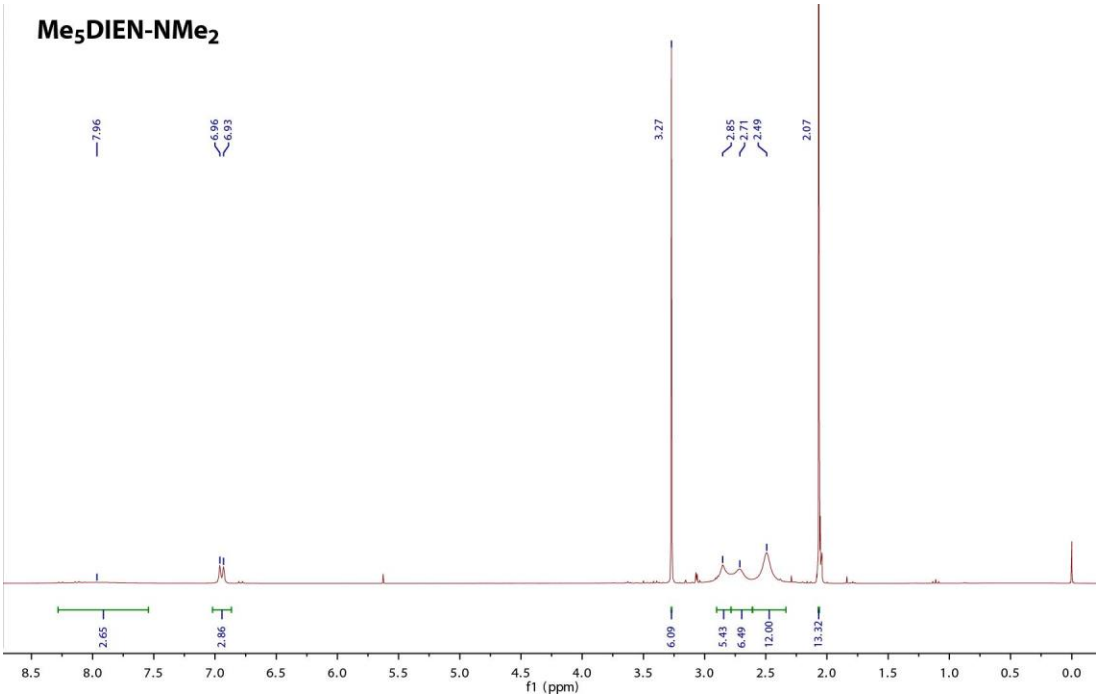

Figure S9. ^{1}H-NMR (500 MHz) spectra of **Me_5DIEN-NMe_2** formed in situ in d^6-acetone at 23°C.

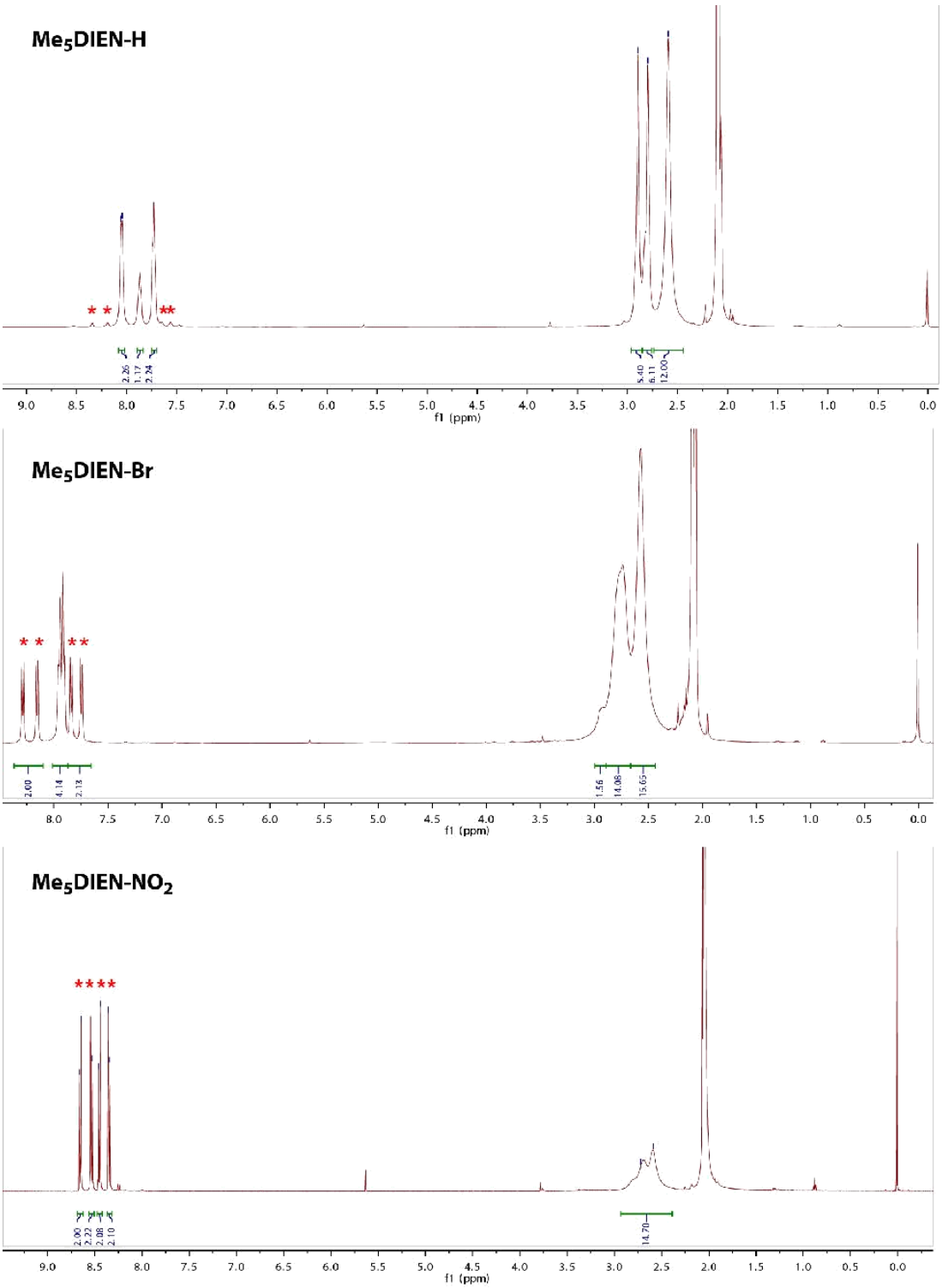

Figure S10. ^{1}H-NMR (500 MHz) spectra of (top to bottom) **Me_5DIEN-H, - Br and -NO_2** formed in situ in d^6- acetone at 23°C, showing the increasing amount of azoxy decomposition product (red *) on going to more electron-poor ArNO moieties.

2.4. Me_6TREN-Z species

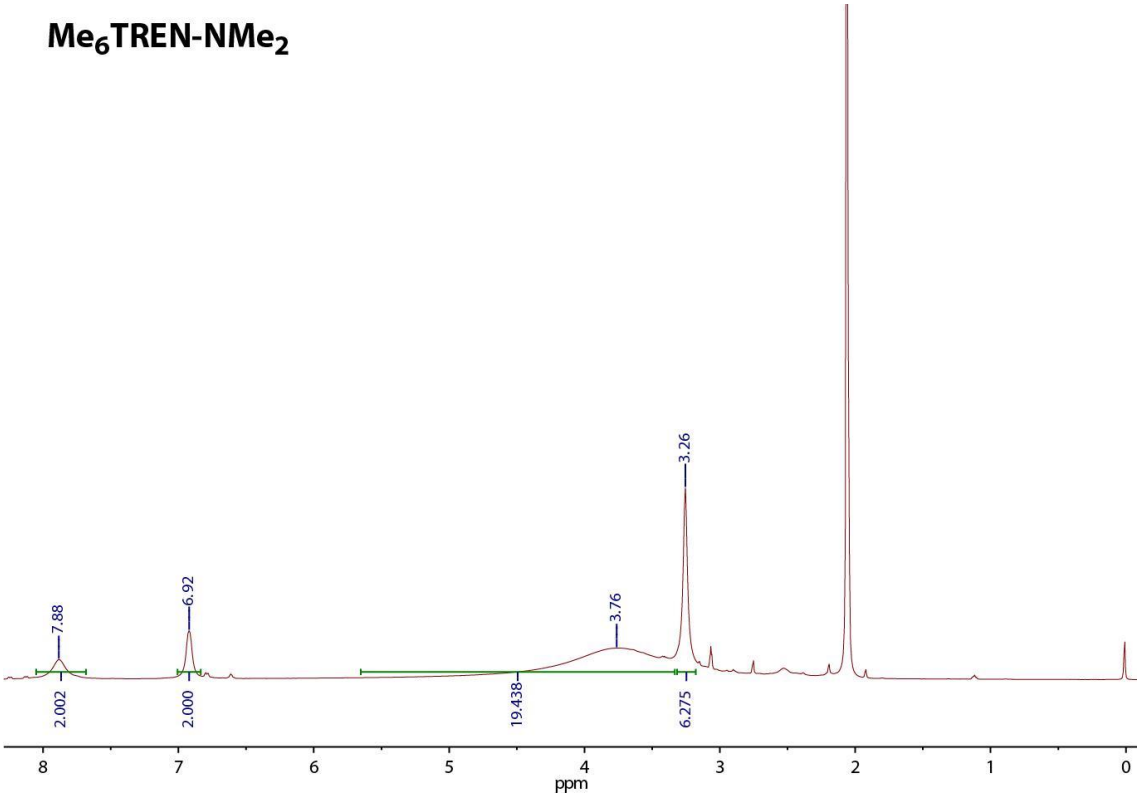

Figure S11. ^{1}H-NMR (500 MHz) spectra of **Me_6TREN-NMe_2** in d^6-acetone at 50°C.

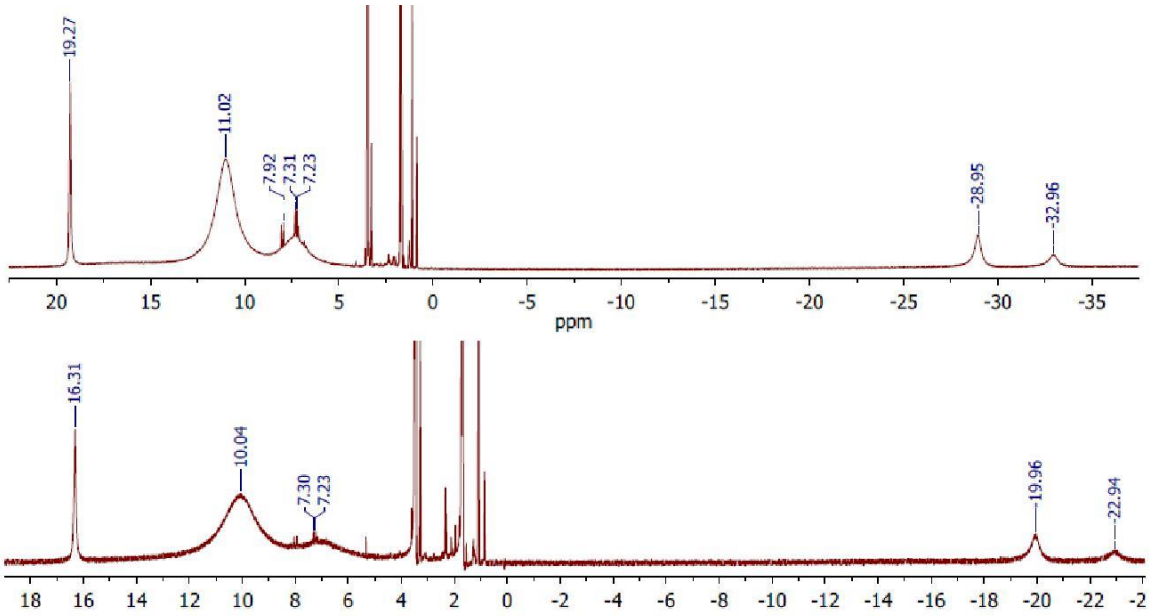

Figure S12. ^{1}H-NMR (500 MHz) spectra of **Me_6TREN-H** with TfO^- (top) or SbF_6^- (bottom) counteranions in d^8-THF at 23°C.

3. X-ray Crystallography

X-ray crystallographyc analysis was performed using the Cu-Kα microfocus or Mo-Kα source of a Bruker APEX-DUO diffractometer or, for **TEED-H**, the Cu-Kα enhanced source of an Oxford Diffraction Gemini A Ultra. The frames were integrated with the Bruker SAINT software package using a narrow-frame algorithm. Data were corrected for absorption effects using the multi-scan method (SADABS or TWINABS). The structures were solved by direct methods and refined using the Bruker APEX2 or APEX3 software package (SHELXL instructions). Non-hydrogen atoms were refined with anisotropic thermal parameters. Hydrogen atoms were generated in idealized positions, riding on the carrier atoms, with isotropic thermal parameters.

Table S1. X-ray crystallographic data for **L-Z** adducts

Adduct name	**DBED-NMe$_2$**	**DBED-H**	**TEED-NMe$_2$**	**Me$_5$DIEN-NMe$_2$**	**Me$_6$TREN-NMe$_2$**	**TEED-H**
Compound	[DBEDCu^{NMe2}ArNO](SbF$_6$)	[DBEDCu^{H}ArNO](SbF$_6$)	[TEEDCu^{NMe2}ArNO](SbF$_6$)	[Me$_5$DIENCu^{NMe2}ArNO](TfO)	[Me$_6$TRENCu^{NMe2}ArNO](TfO)	[TEEDCu(^{H}ArNO)CuTEED](TfO)$_2$
CCDC number	1823004	1823005	1823006	1823007	1823008	1823009
Chemical formula	$C_{18}H_{34}CuF_6N_4OSb\cdot C_4H_8O$	$2(C_{16}H_{29}CuN_3O)\cdot 2(F_6Sb)$	$C_{18}H_{34}CuN_4O\cdot F_6Sb$	$C_{17}H_{33}CuN_5O\cdot CF_3O_3S$	$C_{20}H_{40}CuN_6O\cdot CF_3O_3S$	$C_{27}H_{53}Cu_2F_3N_5O_4S\cdot CF_3O_3S$
M_r	693.88	1157.42	621.78	536.09	593.19	876.95
Crystal system, space group	Monoclinic, $P2_1/n$	Triclinic, $P1$	Monoclinic, $P2_1/c$	Monoclinic, $P2_1/c$	Monoclinic, $P2_1/n$	Monoclinic, $P2_1/c$
Temperature (K)	150	110	150	110	116	100
a (Å)	9.2011 (3)	10.0469 (3)	11.8998 (4)	9.6745 (1)	8.7738 (11)	14.4829 (4)
b (Å)	21.4308 (6)	14.8274 (4)	25.1515 (9)	15.6108 (1)	25.446 (3)	14.6800 (3)
c (Å)	14.8258 (4)	15.8106 (4)	8.3707 (3)	16.0592 (1)	12.7528 (15)	18.7395 (5)
α(°)		108.077 (1)				
β (°)	94.433 (1)	90.643 (2)	97.987 (3)	98.085 (1)	105.723 (7)	107.688 (3)
γ (°)		92.875 (1)				
V (Å^3)	2914.71 (15)	2235.33 (11)	2481.03 (15)	2401.26 (3)	2740.7 (6)	3795.83 (17)
Z	4	2	4	4	4	4
Radiation type	Cu $K\alpha$	Cu $K\alpha$	Cu $K\alpha$	Cu $K\alpha$	Cu $K\alpha$	Cu $K\alpha$
μ (mm^{-1})	8.82	11.32	10.25	2.61	2.35	3.10
Crystal size (mm)	0.31 × 0.17 × 0.12	0.20 × 0.15 × 0.05	0.32 × 0.15 × 0.14	0.16 × 0.14 × 0.08	0.34 × 0.18 × 0.06	0.14 × 0.09 × 0.07
T_{min}, T_{max}	0.492, 0.753	0.356, 0.753	0.407, 0.753	0.667, 0.753	0.617, 0.753	0.880, 1
No. of measured, independent and observed [$I > 2\sigma(I)$] reflections	43477 5344 4774	7984 7984 7434	36450 4552 4099	35778 4408 4063	37557 4990 4536	33632 6625 5038
R_{int}	0.071	0.044	0.095	0.029	0.039	0.054
$(\sin\theta/\lambda)_{max}$ (Å^{-1})	0.603	0.603	0.603	0.603	0.602	0.595
$R[F^2 > 2\sigma(F^2)]$	0.036	0.033	0.034	0.024	0.028	0.073
$wR(F^2)$	0.095	0.073	0.085	0.064	0.074	0.207
Goodness of of fit, S	1.04	1.05	1.05	1.06	1.04	1.11
No. of reflections, parameters, restraints	5344, 333, 0	7984, 517, 0	4552, 286, 0	4408, 296, 0	4990, 333, 0	6625, 470, 0
$\Delta\rho_{max}$, $\Delta\rho_{min}$ (e Å^{-3})	1.09, −0.82	1.26, −0.74	0.69, −1.52	0.29, −0.30	0.34, −0.29	2.59, −1.12
Absolute structure						
Flack parameter						
Selected metrical parameters						
N−O (Å)	1.269	1.236	1.254	1.266	1.260	1.322
Cu−N$_{nitroso}$ (Å)	1.867	1.827-1.828	1.872	1.896	1.934	2.036 (Cu^{II}), 1.885 (Cu^{I})
Cu−O$_{nitroso}$ (Å)						1.880 (Cu^{II}), 2.666 (Cu^{I})
Cu−OTf (Å)						2.266 (Cu^{II}), 2.630 (Cu^{I})
Cu−N$_{ligand}$ (Å)	2.039-2.074	2.004-2.009	2.050-2.058	2.063-2.205	2.095-2.250	2.017-2.019 (Cu^{II}) 2.048-2.130 (Cu^{I})

Table S2. X-ray crystallographic data for other complexes

Adduct name		
Compound	[DBEDCu(∞-DBDI)CuDBED]$(SbF_6)_2$	[TEEDCu(∞-OH)$_2$CuTEED]$(SbF_6)_2$
CCDC number	1823010	1830574
Chemical formula	$C_{30}H_{68}Cu_2N_6 \cdot 2(F_6Sb) \cdot C_4H_8O$	$C_{20}H_{50}Cu_2N_4O_2 \cdot 2(F_6Sb) \cdot C_4H_8O$
M_r	1183.58	1049.36
Crystal system, space group	Monoclinic, $P2_1$	Orthorhombic, *Pmma*
Temperature (K)	150	110
a (Å)	14.7346 (3)	20.2536(5)
b (Å)	10.1121 (2)	13.1606(3)
c (Å)	17.0163 (4)	7.4600(2)
α(°)	90	90
β (°)	101.022 (1)	90
γ (°)	90	90
V (Å^3)	2488.62 (9)	1988.46(9)
Z	2	2
Radiation type	Cu *K*α	Mo *K*α
μ (mm^{-1})	10.15	2.49
Crystal size (mm)	0.36 × 0.06 × 0.06	0.30 × 0.10 × 0.10
T_{min}, T_{max}	0.430, 0.753	0.705, 0.746
No. of measured, independent and observed [$I > 2\sigma(I)$] reflections	34981 8642 8062	12873 2444 2108
R_{int}	0.049	0.036
$(\sin \theta/\lambda)_{max}$ (Å^{-1})	0.604	0.650
$R[F^2 > 2\sigma(F^2)]$	0.027	0.025
$wR(F^2)$	0.055	0.103
Goodness of of fit, *S*	0.98	1.19
No. of reflections, parameters, restraints	8642, 549, 1	2444, 144, 3
$\Delta\rho_{max}$, $\Delta\rho_{min}$ (e Å^{-3})	0.40, −0.59	0.85, −0.78
Absolute structure	Refined as an inversion twin	
Flack parameter	0.010 (5)	
Selected metrical parameters		
Cu···Cu (Å)	5.837	2.997
Cu−OH (Å)		1.923
Cu−N_{ligand} (Å)	2.047-2.064 to DBED 1.903-1.904 to DBDI	2.014

4. DFT details

The theoretical electronic spectra of the analogous *para*-substituted arylnitroso complexes **DBED-Z** and (Z = NMe_2, Br, H, NO_2) were predicted using TD-DFT calculations. All calculations were performed on Gaussian 09[1] using the GGA pure DFT functional BP86 with the triple-zeta polarized Ahlrich basis set Def2TZVP. Geometry optimizations were carried out from x-ray crystal structures using the ultrafine integration grid, tight SCF convergence criteria, and Polarized Continuum Model (PCM) solvent corrections for tetrahydrofuran (ε = 7.6), which was the solvent used to record the compounds' experimental UV-Vis spectra. Using the geometries optimized under implicit solvation, 40 singlet excited states were calculated for each compound using TD-DFT at the same level of theory. Theoretical fits of the UV-Vis spectra were plotted based on the 40 calculated excited states, and Electron Density Difference (EDD) plots were generated for each transition associated with the most intense predicted excited state in the visible range, not including de-excitations or excitations with small or negative CI expansion coefficients.

A sample input section for each type of calculation is provided below:

<u>Geometry Optimization</u>:

```
# bp86/Def2TZVP opt nosymm int=grid=ultrafine
scf=tight scrf=(solvent=tetrahydrofuran)

geometry optimization with implicit solvation

1 1
```

<u>Excited State Calculation</u>:

```
# td=(nstates=40) bp86/def2TZVP nosymm int=grid=ultrafine scf=tight

geom=check TDDFT without scrf=solvent=thf

1 1
```

4.1. DBED-NMe$_2$

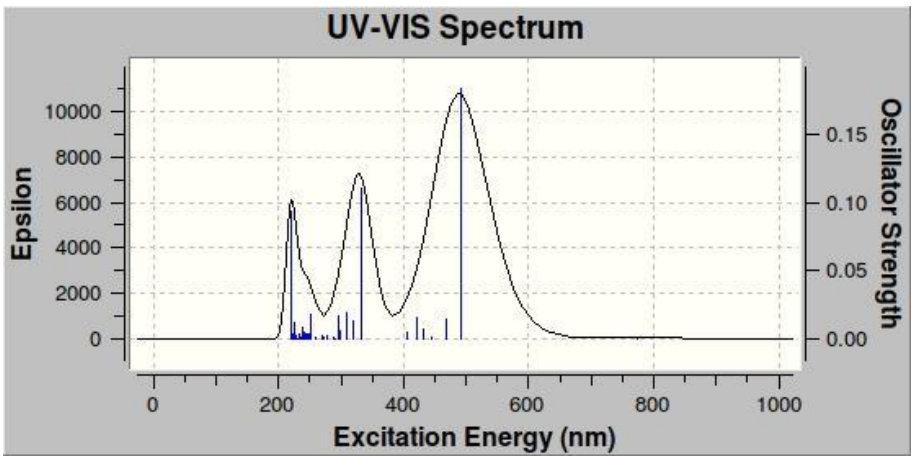

Figure S13. Calculated UV-vis spectrum for **DBED-NMe$_2$**.

Table S3. Transitions involved in the 507.61 nm peak (excited state #2) for **DBED-NMe$_2$**.

Transition	Orbitals Involved	CI expansion Coefficient	Assignment
101 → 104	HOMO-2 → LUMO	0.12349	MLCT
102 → 104	**HOMO-1 → LUMO**	**0.68949**	**MLCT**
102 ← 104	HOMO-1 ← LUMO	-0.12183	

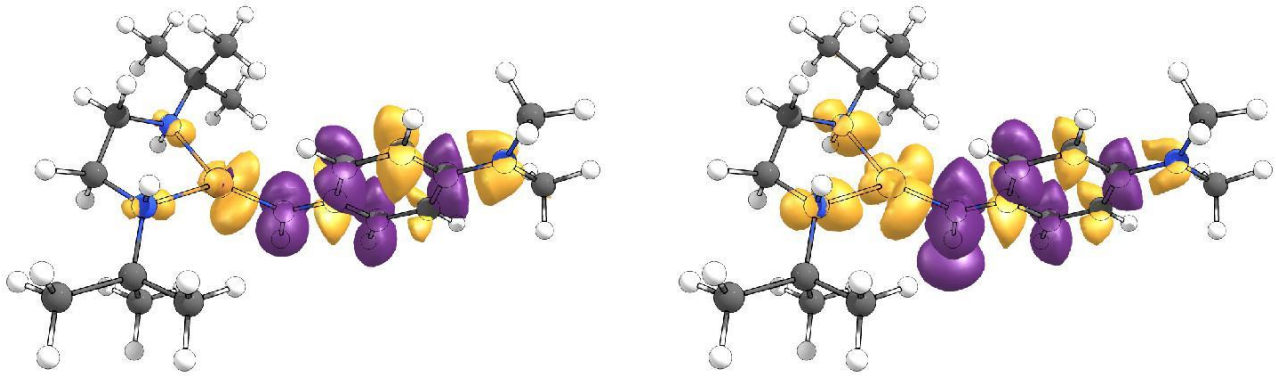

Figure S14. EDD plot of absolute value of 104-101 (left) and 140-102 (right) for **DBED-NMe$_2$**. Purple = (+), yellow = (-).

4.2. DBED-H

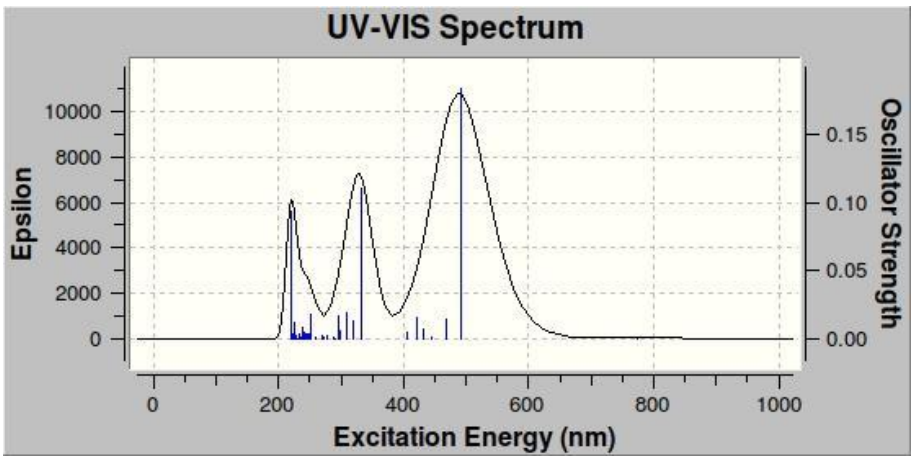

Figure S15. Calculated UV-vis spectrum for **DBED-H**.

Table S4. Transitions involved in the 491.31 nm peak (excited state #2) for **DBED-H**.

Transition	Orbitals Involved	CI expansion Coefficient	Assignment
83 → 92	HOMO-8 → LUMO	0.11167	
85 → 92	HOMO-6 → LUMO	0.10364	
89 → 92	HOMO-2 → LUMO	-0.15051	
90 → 92	**HOMO-1 → LUMO**	**0.67080**	**MLCT**
90 ← 92	HOMO-1 ← LUMO	-0.13135	

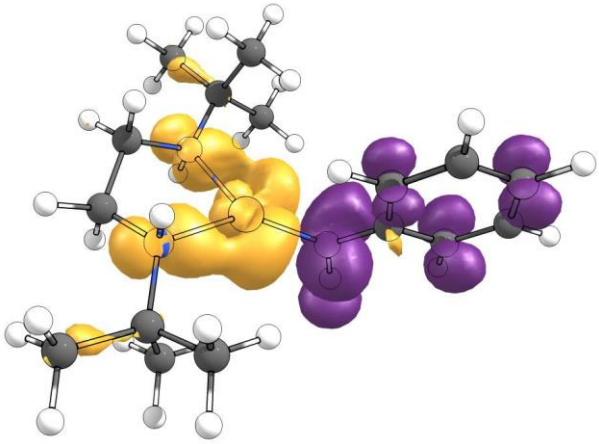

Figure S16. EDD plot of absolute value of 92-90 for **DBED-H**. Purple = (+), yellow = (-).

4.3. DBED-Br

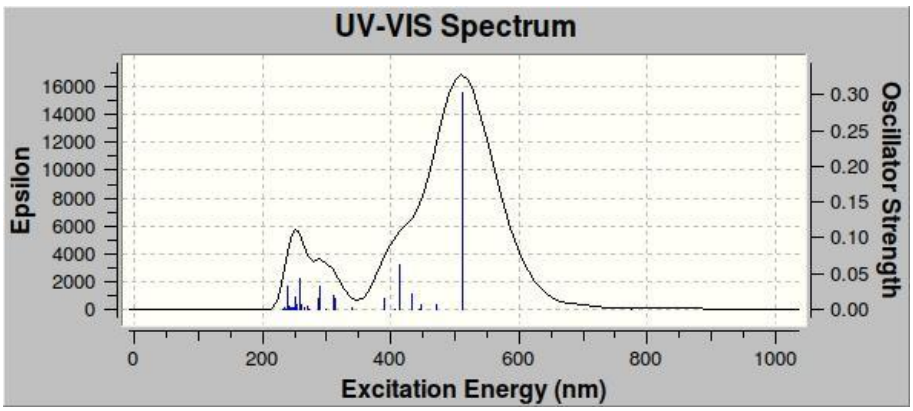

Figure S17. Calculated UV-vis spectrum for **DBED-Br**.

Table S5. Transitions involved in the 512.53 nm peak (excited state #2) for **DBED-Br**.

Transition	Orbitals Involved	CI expansion Coefficient	Assignment
106 → 109	HOMO-2 → LUMO	0.15535	LMCT
107 → 109	**HOMO-1 → LUMO**	**0.67634**	**MLCT**
107 ← 109	HOMO-1 ← LUMO	-0.12520	

Interestingly, **DBED-Br** is an exception to the MLCT assignment, compared with the other species. Its most intense visible excited state includes important contribution from both MLCT and LMCT component transitions, with the second most important contributor identified by EDD plots as an LMCT from HOMO-2 → LUMO (see below).

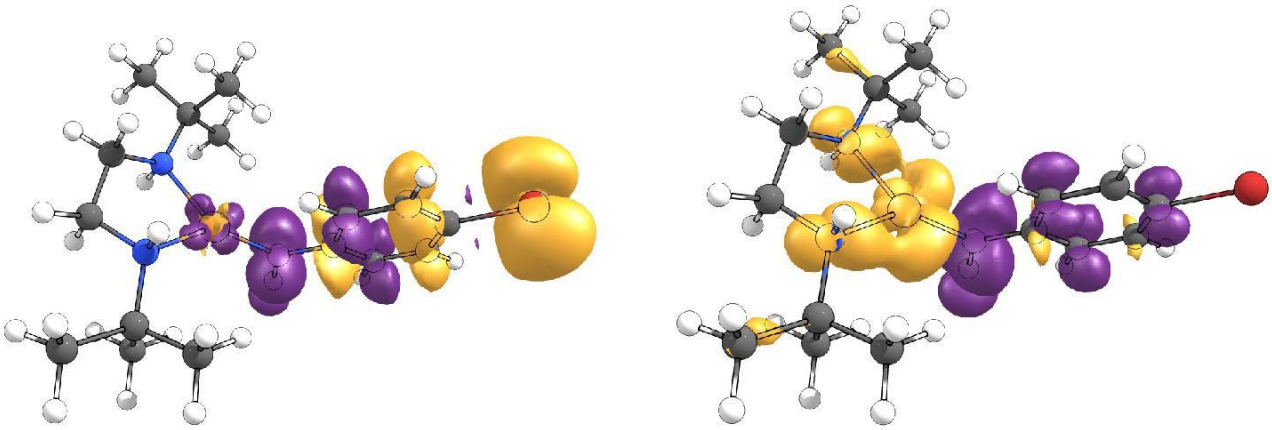

Figure S18. EDD plot of absolute value of 109-106 (left) and 109-107 for **DBED-Br** (right). Purple = (+), yellow = (-).

4.4. DBED-NO_2

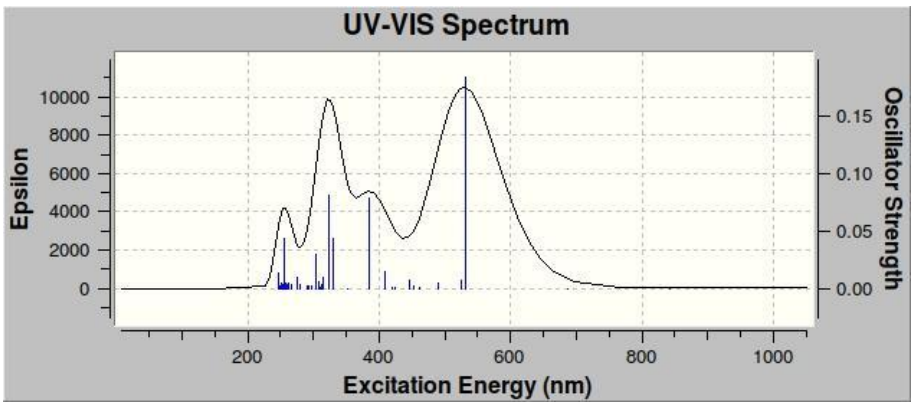

Figure S19. Calculated UV-vis spectrum for **DBED-NO_2**.

Table S6. Transitions involved in the 531.58 nm peak (excited state #2) for **DBED-NO_2**.

Transition	Orbitals Involved	CI expansion Coefficient	Assignment
99 → 103	HOMO-3 → LUMO	-0.11235	
101 → 103	**HOMO-1 → LUMO**	**0.66326**	**MLCT**
101 → 104	HOMO-1 → LUMO+1	0.17260	MLCT
101 ← 103	HOMO-1 ← LUMO	-0.13253	

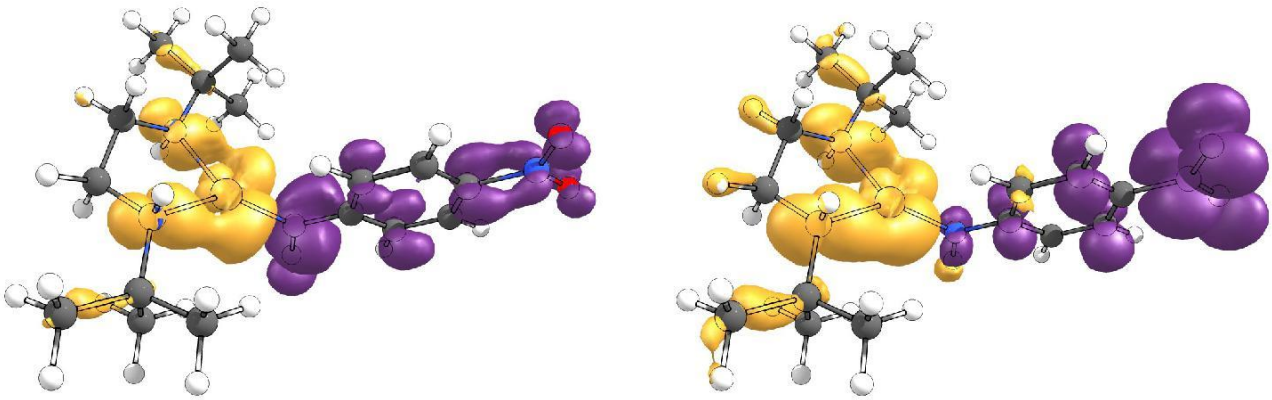

Figure S20. EDD plot of absolute value of 103-101 (left) and 104-101 (right) for **DBED-NO_2**. Purple = (+), yellow = (-).

5. Reference

1. M. J. Frisch, G. W. Trucks, H. B. Schlegel, G. E. Scuseria, M. A. Robb, J. R. Cheeseman, G. Scalmani, V. Barone, B. Mennucci, G. A. Petersson, H. Nakatsuji, M. Caricato, X. Li, H. P. Hratchian, A. F. Izmaylov, J. Bloino, G. Zheng, J. L. Sonnenberg, M. Hada, M. Ehara, K. Toyota, R. Fukuda, J. Hasegawa, M. Ishida, T. Nakajima, Y. Honda, O. Kitao, H. Nakai, T. Vreven, J. J. A. Montgomery, J. E. Peralta, F. Ogliaro, M. Bearpark, J. J. Heyd, E. Brothers, K. N. Kudin, V. N. Staroverov, T. Keith, R. Kobayashi, J. Normand, K. Raghavachari, A. Rendell, J. C. Burant, S. S. Iyengar, J. Tomasi, M. Cossi, N. Rega, J. M. Millam, M. Klene, J. E. Knox, J. B. Cross, V. Bakken, C. Adamo, J. Jaramillo, R. Gomperts, R. E. Stratmann, O. Yazyev, A. J. Austin, R. Cammi, C. Pomelli, J. W. Ochterski, R. L. Martin, K. Morokuma, V. G. Zakrzewski, G. A. Voth, P. Salvador, J. J. Dannenberg, S. Dapprich, A. D. Daniels, O. Farkas, J. B. Foresman, J. V. Ortiz, J. Cioslowski and D. J. Fox, *Gaussian 09, Revision B.01*, (2010) Gaussian, Inc., Wallingford CT.